JTE HCMUTE
ISSN: 2615-9740

JOURNAL OF TECHNICAL EDUCATION SCIENCE
Ho Chi Minh City University of Technology and Education
Website: https://jte.edu.vn
Email: jte@hcmute.edu.vn

A Moving Kriging-Based Meshfree Approach for Vibration Analysis of Functionally Graded TPMS Nanoplate

Lieu Nguyen Thi Bich*
Ho Chi Minh City University of Technology and Education, Vietnam

*Corresponding author. *Email: lieuntb@hcmute.edu.vn*

ARTICLE INFO

Received: 23/05/2025
Revised: 10/06/2025
Accepted: 14/07/2025
Published: 28/11/2025

KEYWORDS

Functionally Graded Nanoplate;
Moving Kriging-Based Meshfree;
Triply periodic minimal surface (TPMS);
Eringen's elasticity theory;
Higher-order shear deformation theory (HSDT).

ABSTRACT

Triply Periodic Minimal Surfaces (TPMS) constitute a novel class of architected materials characterized by three-dimensionally periodic geometries derived from minimal surface mathematics. These materials exhibit a unique combination of low density and high mechanical efficiency, making them highly suitable for applications that demand optimized strength-to-weight performance. Due to their continuous, smoothly curved surfaces and topological complexity, TPMS structures have emerged as promising candidates for use in fields such as biomedical engineering, lightweight structural design, and energy absorption systems. TPMS architectures can be realized through two primary strategies: either by thickening the minimal surface to form sheet-based structures or by solidifying the enclosed volume to generate skeletal or solid-based configurations. This study explores the size effect on the free vibration responses of functionally graded (FG) nanoplates with triply periodic minimal surface (TPMS) design. By employing the higher-order shear deformation theory (HSDT) with five unkown variables, in combination with the moving Kriging meshfree method and incorporating nonlocal Eringen's elasticity theory, we examine two kinds of porous nanostructures: Primitive and Gyroid patterns. For each pattern, four distinct volume dispersal scenarios are considered. The mechanical properties, including elastic modulus, shear modulus, and Poisson's ratio-are obtained through a curve-fitting approach using a two-phase piecewise model. The numerical findings are rigorously compared with reference data from existing literature, ensuring the accuracy of the results.

Doi: https://doi.org/10.54644/jte.2025.1909

1. Introduction

A lot of study has focused on the mechanical properties of common cellular structures such foams, lattices, and honeycombs [1]. Triply periodic minimum surfaces (TPMS) are distinguished from other types by their smooth, continuous forms that can be generated through mathematical formulae. Primitive, Gyroid, and I-WP are examples of typical TPMS types that can be constructed using implicit functions [2]. Thanks to additive printing, these complex shapes can now be produced precisely, allowing scientists to carefully study how they deform and absorb energy. Recent studies have used both models and experiments to examine the mechanical behavior of 3D-printed TPMS structures [3]. Different types of FG-TPMS structures have been created in recent findings to improve the mechanical characteristics of TPMS structures. These structures include gradient volume content [4,5] and hybridization of several unit cell geometries. Gradient-based Primitive and Gyroid configurations have been created by introducing z-dependent terms into the mathematical formulations of TPMS, resulting in functionally graded (FG) structures [6]. It has been demonstrated that these FG structures, which are graded precisely along the build (z) direction, perform better in terms of energy absorption capacity than their uniform counterparts. A hybrid deformation mode that combines behavior dominated by both stretching and bending has been observed in a variety of FG-TPMS architectures that have been investigated [7].

TPMS, also known as crystal structures, are distinguished by their fundamental property of minimal surfaces, non-self-intersecting geometries that effectively reduce stress concentration. This unique characteristic makes these complex porous structures highly advantageous, offering exceptional strength-to-weight ratios and versatile manufacturing potential, which underpin their wide range of practical applications. Maskery et al. [8] examined the mechanical response of these TPMS structures under compressive loading through experimental tests and finite element analysis (FEA). Sychov and his team [9] the mechanical behavior of four different TPMS configurations: Shwartz Diamond, D-prime surface, Neovius surface, and Gyroid, utilizing experimental methodologies. In a different study, Kurup and Pitchaimani [10] introduced the linear aeroelastic flutter analysis of TPMS Euler-Bernoulli beams with four TPMS morphologies: Primitive, Gyroid, Diamond, and I-graph—along with the wrapped package-graph (IWP). Simsek et al. [11] utilized both finite element analysis and experimental approaches to investigate the modal behavior of additively manufactured TPMS beam structures, emphasizing Diamond, Gyroid, IWP, and Primitive unit cells.

The synergistic application of minimal surface architecture and functional material gradation has significantly contributed to the advancement of functionally graded triply periodic minimal surface (FG-TPMS) structures. These have emerged as versatile solutions applicable across diverse fields such as biomechanics, advanced engineering, and materials science. Viet and his team [12], using Euler beam theory and finite element analysis (FEA), introduced the buckling behavior and vibrational properties in FG-TPMS beam configurations, incorporating IWP, Gyroid, Diamond, and Primitive unit cells. In a similar vein, Ejeh et al. [13] explored the influence of relative density gradation and lattice hybridization on the specific flexural properties of four-point loaded beams made from sheet-based TPMS cellular structures. Afshar and his team [14] investigated the deformation mechanisms of TPMS structures with graded porosities, emphasizing the enhanced mechanical properties of structures predominantly characterized by stretching compared to those defined by bending. Moreover, Ma et al. [15] conducted an assessment of the biological and mechanical properties of graded porous scaffolds through the application of sophisticated, Gyroid, Diamond TPMS designs, IWP, and Primitive. Nguyen-Xuan et al. [16] introduced a novel modeling strategy for FG-TPMS plates, which included a unified framework for Gyroid, Primitive, and IWP forms. Their approach was based on a dual-phase density function designed to predict effective material parameters. Building on this work, Nguyen et al. [17] applied the same model to analyze FG-TPMS microplates, employing the modified couple stress theory and isogeometric approach.

Numerous theoretical frameworks have been developed to better understand nanostructures materials. These include Mindlin’s strain gradient theories (first- and second-order), couple stress theory, modified couple stress theory, and elasticity-based formulations such as Eringen’s nonlocal elasticity theory. Key studies employing Eringen's nonlocal theory include Ebrahimi and Salari [18], who investigated the thermo-electrical coupling and buckling properties of FG piezoelectric Timoshenko nanobeams using Navier-type solutions and Eringen’s elasticity theory; Zenkour and Aljadani [19], who analyzed the thermo-electrical buckling of FG piezoelectric nanoplates using refined hyperbolic higher-order shear deformation theory (HSDT) in conjunction with Eringen’s nonlocal theory; and Daneshmehr et al. [20], who explored a size-dependent functionally graded nanoplate. However, despite these advancements, applying the moving Kriging meshfree method to FG-TPMS nanostructures, utilizing nonlocal elasticity theory, remains limited in several areas of research.

This study seeks to explore the free vibration behaviors of FG-TPMS nanoplates through a hybrid numerical approach, combining HSDT and Eringen’s nonlocal elasticity model. To accurately capture higher-order derivatives of approximate variables in weak formulations, it is essential to employ a numerical method that preserves the higher-order continuity of basic functions. To fulfill the requirements of modeling TPMS (Triply Periodic Minimal Surface) nanostructures, this study employs the moving Kriging (MK) meshfree method. The application of MK to TPMS materials represents a novel and original contribution to the field. Owing to the higher-order continuity inherent in MK interpolation functions, the proposed framework is particularly well-suited for analyzing TPMS nanoplates, where third-order derivatives of field variables are involved. Furthermore, unlike many traditional meshfree approaches that rely on Lagrange multipliers or penalty techniques to impose boundary conditions, the MK method allows for the direct enforcement of boundary conditions at nodal

points, analogous to the finite element method (FEM). Originally introduced by Gu [21] for solving two-dimensional boundary value problems, the MK interpolation technique has since been extended and applied to the analysis of plate structures in various studies [22–26]. By combining the MK meshfree method with HSDT, the research provides an integrated approach for analyzing functionally graded triply periodic minimal surface nanostructures. A numerical case study is also provided to highlight the advantages of applying this nonlocal meshfree strategy to such configurations.

2. Primary formulations

2.1. Mechanical characteristics of FG-TPMS materials

In this study, two representative TPMS geometries, namely Primitive (Pri) and Gyroid (Gy), are modeled as follows: [2]:

- Pri: $\phi(x,y,z)=\cos(\kappa_1 x)+\cos(\kappa_2 y)+\cos(\kappa_3 z)$ (1)
- Gy: $\phi(x,y,z)=\sin(\kappa_1 x)\cos(\kappa_2 y)+\sin(\kappa_2 y)\cos(\kappa_3 z)+\sin(\kappa_3 z)\cos(\kappa_1 x)$

where $\phi(x,y,z)$ symbolizes a surface evaluated at a specified constant value, demonstrating a topology similar to that of a minimal surface, and

$$\kappa_i=\frac{2\pi t_i}{l_i},\quad i=1,2 \tag{2}$$

where t_i and l_i imply the number of unit cells and their corresponding lengths, respectively.

To provide a visual perspective, two representative unit cell configurations, namely Primitive (Pri) and Gyroid (Gy), are outlined in Figure 1.

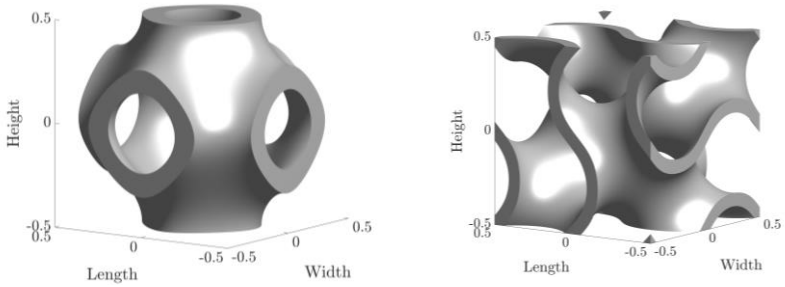

(a) *(b)*

Figure 1. *Different shapes of unit cells: (a) Primitive and (b) Gyroid.*

Regarding the curve-fitting model [2], the volume ratio is determined as follows

$$V=\frac{V^{TPMS}}{V^{m}} \tag{3}$$

in V^m and V^{TPMS} denote the total volume of TPMS base material and cells, respectively.

The V in Eq. (3) can be rewritten as follows:

$$V=(V_{\max}-V_{\min})V_z^{PatternA,B}+V_{\min} \tag{4}$$

where $V_z^{Pattern\ A}=\left(\frac{z}{h}+\frac{1}{2}\right)^n$ and $V_z^{PatternB}=\left(1-\cos\left(\frac{\pi z}{h}\right)\right)^n$.

Regarding Eq. (4), the variation both Pattern A and Pattern B via the plate thickness is represented by using two distinct mathematical purposes.

2.2. Eringen's Nonlocal Elasticity theory

To begin, we analyze a nanoplate structure influenced by a distributed body force field (f_i). The ng equilibrium equation based on a nonlocal linear elastic problem can be expressed:

$$\chi_{ij,j} + f_i = \rho \ddot{u}_i \quad \text{in } \bar{\Omega} \tag{5}$$

where χ_{ij} is the nonlocal stress, $\ddot{u}_i$ is the acceleration field and ρ is the density mass, and $\bar{\Omega}$ is the volume.

In the nonlocal formula proposed by Eringen, the nonlocal stress tensor χ_{ij} can be defined as:

$$\chi_{ij}(\mathbf{x}) = \int_{\bar{\Omega}} \Theta\left(|\mathbf{x}' - \mathbf{x}|, \tau\right) \sigma_{ij}(\mathbf{x}') \mathrm{d}\mathbf{x}' \tag{6}$$

in which $\mathbf{x}$ is a point in the body; $\mathbf{x}'$ is denotes a neighboring point relative to $\mathbf{x}$; $|\mathbf{x}' - \mathbf{x}|$ is measures the space between the points; the kernel function $\Theta\left(|\mathbf{x}' - \mathbf{x}|, \tau\right)$ infers the nonlocal modulus; τ expresses a parameter characterizing the material.

Employing the differential operator $\Xi = \left(1 - \varphi^2 \nabla^2\right)$, Eq. (6) can be modified as [27]

$$\left(1 - \varphi^2 \nabla^2\right) \chi_{ij} = \sigma_{ij} \ , \ \left(1 - \varphi^2 \nabla^2\right) \chi_{ij,j} = \sigma_{ij,j} \tag{7}$$

where the Laplacian operator is defined $\nabla^2 = \dfrac{\partial}{\partial x^2} + \dfrac{\partial}{\partial y^2}$ and φ is the nonlocal parameter; with $\varphi = e_0 a$ accounts for the small-scale effects influencing the behavior of nanostructures, in which e_0 is a material constant and and a denotes the internal characteristic length, accounting for small-scale effects relevant to nanostructure mechanics.

Similarly, Eq. (5) can be reformulated using Ξ. leading to the following form:

$$\Xi(\chi_{ij,j}) + \Xi(f_i) = \Xi(\rho \ddot{u}_i) \text{ in } \bar{\Omega} \tag{8}$$

Substituting Eq. (7) into Eq. (8) to accomplish Eq. (9) is :

$$\sigma_{ij,j} + \left(1 - \varphi^2 \nabla^2\right) f_i = \left(1 - \varphi^2 \nabla^2\right) \rho \ddot{u}_i \tag{9}$$

Using the virtual displacement principle, the integral representation of Eq. (9) is obtained as:

$$\int_{\bar{\Omega}} \sigma_{ij,j} \delta u_i \mathrm{d}\bar{\Omega} + \int_{\bar{\Omega}} \left(1 - \varphi^2 \nabla^2\right) f_i \delta u_i \mathrm{d}\bar{\Omega} = \int_{\bar{\Omega}} \left(1 - \varphi^2 \nabla^2\right) \rho \ddot{u}_i \delta u_i \mathrm{d}\bar{\Omega} \tag{10}$$

where δu_i represents the virtual displacement vector.

Applying the divergence theorem and integration by parts to the first term in Eq. (10), the expression becomes:

$$\int_{\bar{\Omega}} \sigma_{ij,j} \delta u_i \mathrm{d}\bar{\Omega} = -\int_{\bar{\Omega}} \sigma_{ij} \delta u_{i,j} \mathrm{d}\bar{\Omega} + \int_{\Gamma_g} \sigma_{ij} n_i \delta u_i \mathrm{d}\Gamma_g \tag{11}$$

where n_i is normal vector, Γ_g is the Neumann boundary, and $\delta u_{i,j}$ is the derivative of virtual displacement vector.

By substituting Eq. (11) into Eq. (10) and discounting the integrated elements located at the boundary Γ_g, the final integration form of equilibrium equation is calculated as

$$\int_{\bar{\Omega}} \sigma_{ij}\delta u_{i,j}\mathrm{d}\bar{\Omega} + \int_{\bar{\Omega}} \left(1-\varphi^2\nabla^2\right)\rho\ddot{u}_i\delta u_i\mathrm{d}\bar{\Omega} = \int_{\bar{\Omega}} \left(1-\varphi^2\nabla^2\right) f_i\delta u_i\mathrm{d}\bar{\Omega} \tag{12}$$

By replacing $\delta u_{i,j} = \delta\varepsilon_{ij}$, Eq. (12) is reworked as

$$\int_{\bar{\Omega}} \delta\left(\varepsilon_{ij}\right)^T \sigma_{ij}\mathrm{d}\bar{\Omega} + \int_{\bar{\Omega}} \left(1-\varphi^2\nabla^2\right)\rho\delta\left(u_i\right)^T \ddot{u}_i\mathrm{d}\bar{\Omega} = \int_{\bar{\Omega}} \left(1-\varphi^2\nabla^2\right)\delta\left(u_i\right)^T f_i\mathrm{d}\bar{\Omega} \tag{13}$$

2.3. Kinematics of functionally graded triply periodic minimal surface nanoplates

As illustrated in Figure 2, the displacement components at a generic point on the plate, according to HSDT, are expressed as follows:

$$\bar{\mathbf{u}}\left(x,y,z\right) = \mathbf{u}^1\left(x,y\right) + z\mathbf{u}^2\left(x,y\right) + f\left(z\right)\mathbf{u}^3\left(x,y\right) \tag{14}$$

in which

$$\bar{\mathbf{u}} = \begin{Bmatrix}\bar{u}\\ \bar{v}\\ \bar{w}\end{Bmatrix};\ \mathbf{u}^1 = \begin{Bmatrix}u\\ v\\ w\end{Bmatrix};\ \mathbf{u}^2 = -\begin{Bmatrix}w_{,x}\\ w_{,y}\\ 0\end{Bmatrix};\ \mathbf{u}^3 = \begin{Bmatrix}\beta_x\\ \beta_y\\ 0\end{Bmatrix} \tag{15}$$

and *w, u*, and *v* denote in the transverse displacements and in-plane, respectively; β_y and β_x are two rotations of the *x-z, y-z* planes, respectively; the symbols '*,x*' and '*,y*' denote derivative of any function with respect to *x* and *y* directions, respectively; $f\left(z\right) = z - 4z^3/3h^2$, and *h* is represents the thickness of the plate. This aspect is explored in [28].

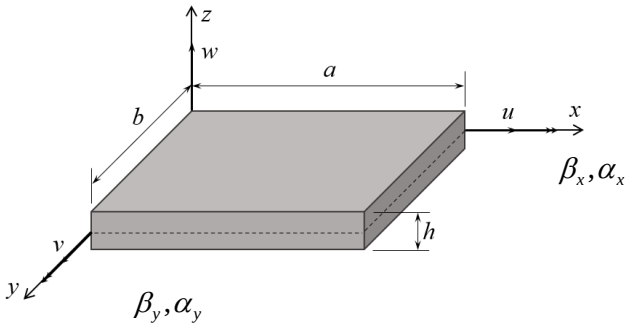

Figure 2. *Elements of the displacement field components.*

Regarding the displacement fields given in Eq. (14), the shear strains and bending can be drawn as:

$$\boldsymbol{\varepsilon} = \left\{\varepsilon_{xx} \quad \varepsilon_{yy} \quad \gamma_{xy}\right\}^{\mathrm{T}} = \boldsymbol{\varepsilon}^1 + z\boldsymbol{\varepsilon}^2 + f\left(z\right)\boldsymbol{\varepsilon}^3;\ \boldsymbol{\gamma} = \left\{\gamma_{xz} \quad \gamma_{yz}\right\}^{\mathrm{T}} = f^{'}\left(z\right)\boldsymbol{\varepsilon}^{\mathrm{s}} \tag{16}$$

in which

$$\boldsymbol{\varepsilon}^1 = \begin{Bmatrix}u_{,x}\\ v_{,y}\\ u_{,y}+v_{,x}\end{Bmatrix};\ \boldsymbol{\varepsilon}^2 = -\begin{Bmatrix}w_{,xx}\\ w_{,yy}\\ 2w_{,xy}\end{Bmatrix};\ \boldsymbol{\varepsilon}^3 = \begin{Bmatrix}\beta_{x,x}\\ \beta_{y,y}\\ \beta_{x,y}+\beta_{y,x}\end{Bmatrix};\ \boldsymbol{\varepsilon}^{\mathrm{s}} = \begin{Bmatrix}\beta_x\\ \beta_y\end{Bmatrix}. \tag{17}$$

and $f'(z) = 1 - 4z^2/h^2$.

For linear elastic materials, the relationship between stress and strain is expressed mathematically by the constitutive law as follows

$$\begin{Bmatrix}\sigma_{xx}\\ \sigma_{yy}\\ \tau_{xy}\\ \tau_{xz}\\ \tau_{yz}\end{Bmatrix}=\begin{bmatrix}\frac{E}{1-\nu^2} & \frac{\nu E}{1-\nu^2} & 0 & 0 & 0\\ \frac{\nu E}{1-\nu^2} & \frac{E}{1-\nu^2} & 0 & 0 & 0\\ 0 & 0 & G & 0 & 0\\ 0 & 0 & 0 & G & 0\\ 0 & 0 & 0 & 0 & G\end{bmatrix}\begin{Bmatrix}\varepsilon_{xx}\\ \varepsilon_{yy}\\ \gamma_{xy}\\ \gamma_{xz}\\ \gamma_{yz}\end{Bmatrix} \tag{18}$$

in which ν, G, and E are the Poisson's ratio, shear modulus, and Young's modulus of FG-TPMS materials, respectively.

Regarding the fixed data model [16], the corresponding values are calculated and listed in Table 1 as follows:

Table 1. *Mechanical characteristics of FG-TPMS materials.*

TPMS	Mechanical characteristics	V Range
Primitive	$E=E^m\begin{cases}0.317V^{1.264}\\ 1.007V^{2.006}-0.007\end{cases};\ G=G^m\begin{cases}0.705V^{1.189}\\ 0.953V^{1.715}+0.047\end{cases}$	$V\le 0.25$ $V>0.25$
	$\nu=\begin{cases}0.314e^{-1.004V}+0.119\\ 0.152V^2-0.235V+0.383\end{cases}$	$V\le 0.55$ $V>0.55$
Gyroid	$E=E^m\begin{cases}0.596V^{1.467}\\ 0.962V^{2.351}+0.038\end{cases};\ G=G^m\begin{cases}0.777V^{1.544}\\ 0.973V^{1.982}+0.027\end{cases}$	$V\le 0.45$ $V>0.45$
	$\nu=\begin{cases}0.192e^{-1.349V}+0.202\\ 0.402V^2-0.603V+0.501\end{cases}$	$V\le 0.50$ $V>0.50$

The discretized governing equations for analyzing nonlocal free vibrations can be formulated by substituting respective components into Eq. (13) as follows:

$$\int_\Omega \delta\bar{\boldsymbol{\varepsilon}}^T\mathbf{Q}^b\bar{\boldsymbol{\varepsilon}}\mathrm{d}\Omega+\int_\Omega \delta\bar{\boldsymbol{\gamma}}^T\mathbf{Q}^s\bar{\boldsymbol{\gamma}}\mathrm{d}\Omega+\int_\Omega\left(1-\varphi^2\nabla^2\right)\delta\bar{\mathbf{u}}^T\mathbf{I}_0\ddot{\bar{\mathbf{u}}}\mathrm{d}\Omega=\mathbf{0} \tag{19}$$

where

$$\bar{\boldsymbol{\varepsilon}}=\begin{Bmatrix}\boldsymbol{\varepsilon}^1\\ \boldsymbol{\varepsilon}^2\\ \boldsymbol{\varepsilon}^3\end{Bmatrix};\ \bar{\boldsymbol{\gamma}}=\left\{\boldsymbol{\varepsilon}^s\right\};\ \mathbf{Q}^b=\begin{bmatrix}\mathbf{A}^b & \mathbf{B}^b & \mathbf{E}^b\\ \mathbf{B}^b & \mathbf{D}^b & \mathbf{F}^b\\ \mathbf{E}^b & \mathbf{F}^b & \mathbf{H}^b\end{bmatrix};$$

$$\left(\mathbf{A}^b,\mathbf{B}^b,\mathbf{D}^b,\mathbf{E}^b,\mathbf{F}^b,\mathbf{H}^b\right)=\int_{-h/2}^{h/2}\left(1,z,z^2,f(z),z\,f(z),f^2(z)\right)\mathbf{C}^b\mathrm{d}z\ ;$$

$$\left(\mathbf{I}_1,\mathbf{I}_2,\mathbf{I}_3,\mathbf{I}_4,\mathbf{I}_5,\mathbf{I}_6\right)=\int_{-h/2}^{h/2}\rho\left(1,z,z^2,f(z),zf(z),f^2(z)\right)\mathbf{I}_{3x3}\mathrm{d}z\,; \tag{20}$$

$$\mathbf{Q}^s=\int_{-h/2}^{h/2}f'^2(z)\mathbf{C}^s\mathrm{d}z;\ \ \mathbf{C}^s=\begin{bmatrix}G & 0\\ 0 & G\end{bmatrix};$$

$$\mathbf{C}^b=\begin{bmatrix}\frac{E}{1-\nu^2} & \frac{\nu E}{1-\nu^2} & 0\\ \frac{\nu E}{1-\nu^2} & \frac{E}{1-\nu^2} & 0\\ 0 & 0 & G\end{bmatrix};\ \bar{\mathbf{u}}=\begin{Bmatrix}\mathbf{u}^1\\ \mathbf{u}^2\\ \mathbf{u}^3\end{Bmatrix};\ \mathbf{I}_0=\begin{bmatrix}\mathbf{I}_1 & \mathbf{I}_2 & \mathbf{I}_4\\ \mathbf{I}_2 & \mathbf{I}_3 & \mathbf{I}_5\\ \mathbf{I}_4 & \mathbf{I}_5 & \mathbf{I}_6\end{bmatrix}$$

where Ω represents a plane surface area of the plate; $\mathbf{I}_{3\times3}$ indicates the unit matrix; $\rho=\rho^m\times V$, in which ρ^m is the mass density of base material.

2.4. Moving Kriging interpolation shape function for FG-TPMS nanoplates

The mid-plane surface is partitioned into a finite set of nodal points $\mathbf{x}_I\,(I=1,..,N)$ and N denotes the total number of nodes. The displacement field is subsequently formulated over this discretized domain.

$$\mathbf{u}^h(\mathbf{x})=\sum_{I=1}^{N}\mathbf{I}_{5\times5}N_I(\mathbf{x})\mathbf{q}_I \tag{21}$$

where $\mathbf{q}_I=\{u_I \quad v_I \quad w_I \quad \beta_{xI} \quad \beta_{yI}\}^T$ is degrees of freedom (DOFs) of node I; the shape function $N_I(\mathbf{x})$ can be formulated

$$N_I(\mathbf{x})=\mathbf{p}^{\mathrm{T}}(\mathbf{x})\mathbf{A}+\mathbf{r}^{\mathrm{T}}(\mathbf{x})\mathbf{B}=\sum_{j=1}^{m}p_j(\mathbf{x})A_{jI}+\sum_{k=1}^{n}r_k(\mathbf{x})B_{kI} \tag{22}$$

in which n corresponds to the count of nodes comprising the support domain, and m signifies the polynomial basis function's order.

And, elements of **p**(**x**), **r**(**x**), **A** and **B** can be written

$$\begin{aligned}\mathbf{p}(\mathbf{x})&=\begin{bmatrix}p_1(\mathbf{x}) & p_2(\mathbf{x}) & \cdots & p_m(\mathbf{x})\end{bmatrix}^T\\ \mathbf{r}(\mathbf{x})&=\begin{bmatrix}R(\mathbf{x}_1,\mathbf{x}) & R(\mathbf{x}_2,\mathbf{x}) & \cdots & R(\mathbf{x}_n,\mathbf{x})\end{bmatrix}^T\\ \mathbf{A}&=\left(\mathbf{S}^{\mathrm{T}}\mathbf{R}^{-1}\mathbf{S}\right)^{-1}\mathbf{S}^{\mathrm{T}}\mathbf{R}^{-1};\ \mathbf{B}=\mathbf{R}^{-1}\left(\mathbf{I}-\mathbf{S}\mathbf{A}\right)\end{aligned} \tag{23}$$

where **I** is a unit matrix of size $n\times n$, and

$$\mathbf{S}(\mathbf{x})=\begin{bmatrix}p_1(\mathbf{x}_1) & \cdots & p_m(\mathbf{x}_1)\\ \vdots & \ddots & \vdots\\ p_1(\mathbf{x}_n) & \cdots & p_m(\mathbf{x}_n)\end{bmatrix};\ \mathbf{R}(\mathbf{x})=\begin{bmatrix}R(\mathbf{x}_1,\mathbf{x}_1) & \cdots & R(\mathbf{x}_1,\mathbf{x}_n)\\ \vdots & \ddots & \vdots\\ R(\mathbf{x}_n,\mathbf{x}_1) & \cdots & R(\mathbf{x}_n,\mathbf{x}_n)\end{bmatrix} \tag{24}$$

with

$$\mathbf{p}(\mathbf{x})=\left\{\underbrace{1 \quad x \quad y \quad x^2 \quad xy \quad y^2}_{m=6}\right\}^T;\ R(\mathbf{x}_i,\mathbf{x}_j)=\exp\left\{-\left(\frac{\zeta}{x_c}\|\mathbf{x}_i-\mathbf{x}_j\|\right)^2\right\} \tag{25}$$

where ζ is a correlation parameter ($\zeta=1$) [2], x_c is mean distance between nodes.

Based on the MK interpolation shape function, shear strain and bending parts can be reformulated as

follows:

$$\bar{\boldsymbol{\varepsilon}}^b = \left\{\boldsymbol{\varepsilon}^1 \quad \boldsymbol{\varepsilon}^2 \quad \boldsymbol{\varepsilon}^3\right\}^T = \sum_{I=1}^{mxn}\left\{\mathbf{B}_I^1 \quad \mathbf{B}_I^2 \quad \mathbf{B}_I^3\right\}^T \mathbf{d}_I = \sum_{I=1}^{mxn}\mathbf{B}_I^b\mathbf{d}_I$$
$$\bar{\boldsymbol{\varepsilon}}_s = \sum_{I=1}^{mxn}\mathbf{B}_I^s\mathbf{d}_I \tag{26}$$

where

$$\mathbf{B}_I^1 = \begin{bmatrix} R_{I,x} & 0 & 0 & 0 & 0 \\ 0 & R_{I,y} & 0 & 0 & 0 \\ R_{I,y} & R_{I,x} & 0 & 0 & 0 \end{bmatrix}, \mathbf{B}_I^2 = -\begin{bmatrix} 0 & 0 & R_{I,xx} & 0 & 0 \\ 0 & 0 & R_{I,yy} & 0 & 0 \\ 0 & 0 & 2R_{I,xy} & 0 & 0 \end{bmatrix}, \mathbf{B}_I^3 = \begin{bmatrix} 0 & 0 & 0 & R_{I,x} & 0 \\ 0 & 0 & 0 & 0 & R_{I,y} \\ 0 & 0 & 0 & R_{I,y} & R_{I,x} \end{bmatrix},$$
$$\mathbf{B}_I^s = \begin{bmatrix} 0 & 0 & 0 & R_I & 0 \\ 0 & 0 & 0 & 0 & R_I \end{bmatrix} \tag{27}$$

In the same way, the displacement field regarding Eq. (15) is also stated by

$$\bar{\mathbf{u}} = \left\{\mathbf{u}^1 \quad \mathbf{u}^2 \quad \mathbf{u}^3\right\}^T = \sum_{I=1}^{mxn}\left\{\mathbf{N}_I^1 \quad \mathbf{N}_I^2 \quad \mathbf{N}_I^3\right\}^T \mathbf{q}_I = \sum_{I=1}^{mxn}\bar{\mathbf{N}}_I\mathbf{q}_I \tag{28}$$

in which

$$\mathbf{N}_I^1 = \begin{bmatrix} R_I & 0 & 0 & 0 & 0 \\ 0 & R_I & 0 & 0 & 0 \\ 0 & 0 & R_I & 0 & 0 \end{bmatrix}, \mathbf{N}_I^2 = -\begin{bmatrix} 0 & 0 & R_{I,x} & 0 & 0 \\ 0 & 0 & R_{I,y} & 0 & 0 \\ 0 & 0 & 0 & 0 & 0 \end{bmatrix}, \mathbf{N}_I^3 = \begin{bmatrix} 0 & 0 & 0 & R_I & 0 \\ 0 & 0 & 0 & 0 & R_I \\ 0 & 0 & 0 & 0 & 0 \end{bmatrix} \tag{29}$$

Finally, discrete equations of free vibration of FG-TPMS nanoplates are devised by inserting Eqs. (26) and (28) into Eq. (19) as follows

$$\left(\mathbf{K} - \omega^2\mathbf{M}\right)\bar{\mathbf{q}} = \mathbf{0} \tag{30}$$

in which $\mathbf{M}$ and $\mathbf{K}$ are the mass matrix and global stiffness matrix, respectively, that are formulated by

$$\mathbf{K} = \int_\Omega \left(\mathbf{B}^b\right)^T \mathbf{Q}^b\mathbf{B}^b d\Omega + \int_\Omega \left(\mathbf{B}^s\right)^T \mathbf{Q}^s\mathbf{B}^s d\Omega;$$
$$\mathbf{M} = \int_\Omega \left(1 - \varphi\nabla^2\right)^T \bar{\mathbf{N}}^T\mathbf{I}_0\bar{\mathbf{N}} d\Omega; \quad \mathbf{q} = \bar{\mathbf{q}}e^{i\omega t} \tag{31}$$

where ω and $\bar{\mathbf{q}}$ are the natural frequency and shape modes of ω, respectively.

3. Validation through numerical simulations

Each category of FG-TPMS plate is demonstrated through a numerical example, considering four distinct volume distribution scenarios $V_{average} = 0.35$ based on Eq. (4), as drawn in Table 2. Three-node triangular cells are employed to carry out the required integration within the meshfree framework, with a specified number of integration points 3×3 assigned to each triangular cell.

The physical properties of SUS304 steel can be described by, $\rho^m = 8000$ kg/m^3, $v^m = 0.3$, and $E^m = 200$ GPa.

JTE HCMUTE
ISSN: 2615-9740
JOURNAL OF TECHNICAL EDUCATION SCIENCE
Ho Chi Minh City University of Technology and Education
Website: https://jte.edu.vn
Email: jte@hcmute.edu.vn

Table 2. *The four cases of volume dispersion characteristics with* $V_{average}$ *= 0.35* [2].

Parameters	n	V_{min}	V_{max}
A1	1	0.2	0.5
A2	3	0.2	0.8
B1	0.561	0.2	0.5
B2	1.757	0.2	0.8

We analyze a square nanoplate with dimensions characterized by length *a* and thickness *h*, subjected to both simply supported (SSSS) and fully clamped (CCCC) boundary conditions. To confirm the accuracy of the proposed model, we initially investigated how different thickness-to-length ratios, TPMS model variants, volume dispersion schemes, and boundary conditions affect the natural frequencies. The expression used to estimate the non-dimensional natural frequency is given by: $\bar{\omega} = \left(\frac{\omega^2 a^4 \rho^m h}{D} \right)^{1/4}$, where $D = \frac{E^m h^3}{12\left(1-\left(v^m\right)^2\right)}$.

The dimensionless natuTable 3ral frequency of FG-TPMS square nanoplate models was computed using 468 nodes. presents the outcomes for the fundamental frequency of FG-TPMS plates without incorporating the nonlocal effect. These outcomes are evaluated against previous studies [16], which employed IGA alongside seventh-order shear deformation theory, as well as the work of Phung et al. [28], which utilized IGA and third-order shear deformation theory. The comparison reveals a strong agreement with these reference solutions [16,28], particularly in scenarios where size-dependent effects are neglected.

Furthermore, Table 3 illustrates a significant increase in the fundamental frequency when transitioning from the Gyroid to the Primitive topology in Pattern A. This ascending trend in frequency is attributed to the variation in structural characteristics between these TPMS forms. The observed upward trend in natural frequency persists as the structural configuration transitions from Pattern A to Pattern B. Notably, the frequency parameters exhibit an increasing tendency with higher length-to-thickness ratios, while a reduction is observed under a change in boundary conditions from CCCC to SSSS. Furthermore, the effect of nonlocal parameters on the fundamental frequency of the nanoplate is systematically investigated, with the corresponding results summarized in Table 4. These results offer novel insights not previously stated in several studies. Notably, the initial frequency is found to be lower in Pattern *A* than in Pattern *B*. In addition, a rise in the nonlocal parameter corresponds to a decrease in the initial frequency, indicating that such parameters effectively reduce structural stiffness. Furthermore, Figure 3 shows the first four our vibration modes of a fully clamped FG-TPMS square nanoplate with a thickness ratio *a*/*h*=10, initial nonlocal parameter $e_0 = 0.5$, Primitive geometry, and Pattern A distribution.

Table 3. *The fundamental non-dimensional natural frequency* $\bar{\omega}$ *of FG-TPMS square plates.*

Thickness-to-length ratios	Triply periodic minimum surfaces	Refs.	Pattern *A*		Pattern *B*	
			A1	A2	B1	B2
SSSS						
10	Pri	Phung et al. [28]	3.4831	3.5445	3.8500	4.1699
		Nguyen et al. [16]	3.4826	3.5452	3.8517	4.1759
		Present	3.4846	3.5459	3.8516	4.1717
	Gy	Phung et al. [28]	3.4049	3.4713	3.7153	4.0314

		Nguyen et al. [16]	3.4047	3.4726	3.7183	4.0429
		Present	3.4068	3.4731	3.7171	4.0331
200	Pri	Nguyen et al. [16]	3.5274	3.5965	3.9322	4.3050
		Present	3.5513	3.6201	3.9511	4.3213
	Gy	Nguyen et al. [16]	3.4553	3.5317	3.8090	4.1968
		Present	3.4751	3.5519	3.8255	4.2116
CCCC						
10	Pri	Phung et al. [28]	4.4396	4.4980	4.9017	5.2641
		Nguyen et al. [16]	4.4454	4.5076	4.9193	5.2988
		Present	4.4442	4.5029	4.9061	5.2689
	Gy	Phung et al. [28]	4.4326	4.5098	4.7493	5.0528
		Nguyen et al. [16]	4.4413	4.5241	4.7741	5.1064
		Present	4.4361	4.5138	4.7532	5.0578
200	Pri	Nguyen et al. [16]	4.5914	4.6724	5.1894	5.7319
		Present	4.6851	4.7663	5.2624	5.7948
	Gy	Nguyen et al. [16]	4.6208	4.7332	5.0902	5.6285
		Present	4.6925	4.8068	5.1510	5.6834

Table 4. *Fundamental non-dimensional natural frequency $\bar{\omega}$ of FG-TPMS square nanoplates for a/h=10.*

e_0	Triply periodic minimum surfaces	Pattern *A*		Pattern *B*	
		A1	**A2**	**B1**	**B2**
SSSS					
0	Pri	3.4846	3.5459	3.8516	4.1717
	Gy	3.4068	3.4731	3.7171	4.0331
0.2	Pri	3.0121	3.0650	3.3293	3.6060
	Gy	2.9448	3.0022	3.2131	3.4863
0.5	Pri	2.2316	2.2708	2.4667	2.6717
	Gy	2.1818	2.2243	2.3805	2.5830
0.8	Pri	1.8125	1.8444	2.0035	2.1701
	Gy	1.7721	1.8066	1.9336	2.0980
1	Pri	1.6320	1.6607	1.8040	1.9540
	Gy	1.5957	1.6267	1.7410	1.8891
CCCC					
0	Pri	4.4442	4.5029	4.9061	5.2689
	Gy	4.4361	4.5138	4.7532	5.0578
0.2	Pri	3.7555	3.8052	4.1517	4.4676
	Gy	3.7498	3.8164	4.0263	4.2959
0.5	Pri	2.7230	2.7590	3.0118	3.2439
	Gy	2.7185	2.7670	2.9220	3.1223
0.8	Pri	2.1997	2.2288	2.4330	2.6208
	Gy	2.1959	2.2350	2.3606	2.5228
1	Pri	1.9778	2.0039	2.1875	2.3564
	Gy	1.9743	2.0095	2.1224	2.2684

JTE
HCMUTE
ISSN: 2615-9740

JOURNAL OF TECHNICAL EDUCATION SCIENCE
Ho Chi Minh City University of Technology and Education
Website: https://jte.edu.vn
Email: jte@hcmute.edu.vn

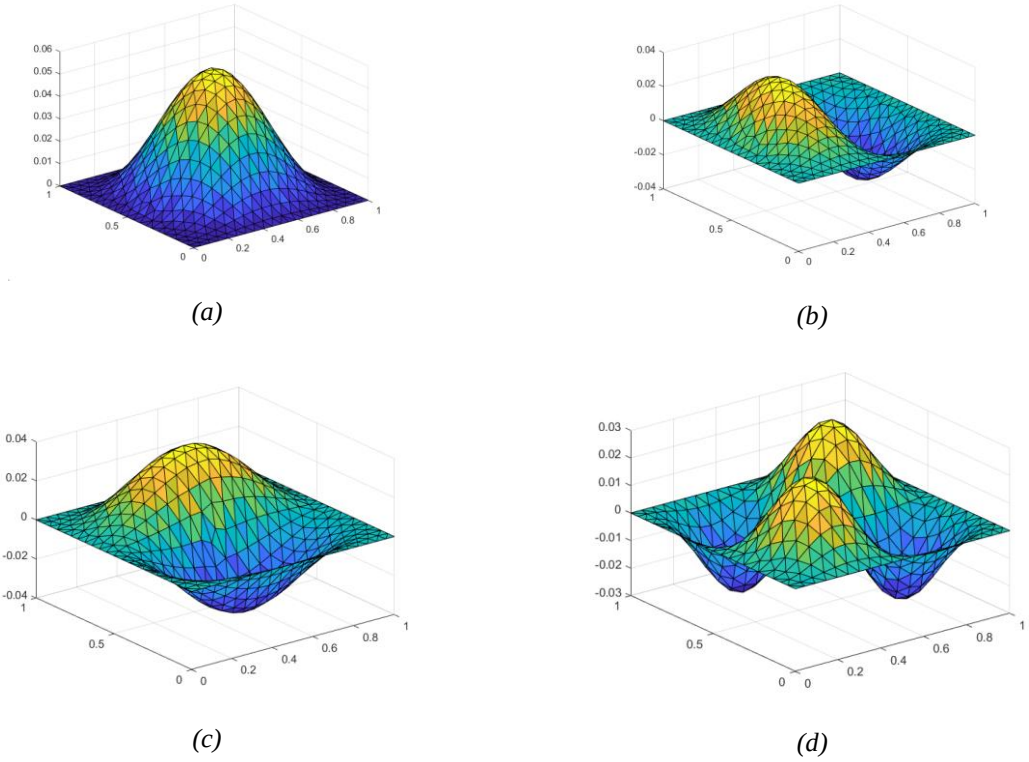

(a) *(b)*

(c) *(d)*

Figure 3. *The first four shape modes of fully clamped FG-TPMS nanoplate (Primitive, Pattern A, a/h=10,* $e_0 = 0.5$ *): (a) Mode 1, (b) Mode 2, (c) Mode 3, and (d) Mode 4.*

4. Conclusions

This study investigated the free vibration behavior of functionally graded triply periodic minimal surface (FG-TPMS) nanoplates using a meshfree model based on higher-order shear deformation theory (HSDT) combined with the moving Kriging method. Two types of TPMS geometries (Primitive and Gyroid) were considered, each featuring four different volume fraction distributions. The mechanical behavior of the FG-TPMS materials was determined using a two-phase piecewise approximation function. The meshfree model produced results that closely matched those reported in the reference literature. Additionally, the influence of stiffness variation on the nanoplates was investigated.

The findings revealed that increasing the nonlocal parameter reduced the natural frequencies of the FG-TPMS nanoplates. Physically, this trend reflects the size-dependent behavior inherent in nanoscale materials: as the nonlocal effect becomes more pronounced, the material exhibits softer mechanical responses due to long-range interatomic interactions. This is particularly relevant for nano-engineered materials where classical continuum theories fail to capture scale effects.

The observation that type A nanoplates have lower fundamental frequencies than type B implies that the stiffness distribution in type A is less favorable for vibration resistance. This has direct implications for structural design, suggesting that certain gradation patterns (e.g., type B) could enhance stiffness without increasing material usage. Furthermore, the Primitive geometry showing the highest first natural frequency indicates a superior ability to resist dynamic loads, making it more suitable for applications where high rigidity and vibrational stability are critical—such as in nanosensors, aerospace components, or micro-electromechanical systems (MEMS).

Overall, these insights provide valuable guidelines for optimizing the design of FG-TPMS nanostructures, balancing material gradation, geometry, and scale effects to meet specific performance demands in advanced engineering applications.

Conflict of Interest

The authors declare no conflict of interest.

Data Availability Statement

The data that support the findings of this study are available from the corresponding author upon reasonable request.

REFERENCES

[1] Y. Sun and Q. M. Li, "Dynamic compressive behaviour of cellular materials: A review of phenomenon, mechanism and modelling," *Int. J. Impact Eng.*, vol. 112, pp. 74–115, 2018.
[2] I. Maskery, L. Sturm, A. O. Aremu, A. Panesar, C. B. Williams, and C. J. Tuck, "Insights into the mechanical properties of several triply periodic minimal surface lattice structures made by polymer additive manufacturing," *Polymer*, vol. 152, pp. 62–71, 2018.
[3] O. Al-Ketan, D. W. Lee, R. Rowshan, and R. K. A. Al-Rub, "Functionally graded and multimorphology sheet TPMS lattices: Design, manufacturing, and mechanical properties," *J. Mech. Behav. Biomed. Mater.*, vol. 102, p. 103520, 2020.
[4] M. Afshar, A. P. Anaraki, H. Montazerian, and J. Kadkhodapour, "Additive manufacturing and mechanical characterization of graded porosity scaffolds designed based on triply periodic minimal surface architectures," *J. Mech. Behav. Biomed. Mater.*, vol. 62, pp. 481–494, 2016.
[5] L. Cheng, J. Bai, and A. C. To, "Functionally graded lattice structure topology optimization for the design of additive manufactured components with stress constraints," *Comput. Methods Appl. Mech. Eng.*, vol. 344, pp. 334–359, 2019.
[6] F. P. W. Melchels, K. Bertoldi, R. Gabbrielli, A. H. Velders, J. Feijen, and D. W. Grijpma, "Mathematically defined tissue engineering scaffold architectures prepared by stereolithography," *Biomaterials*, vol. 31, no. 27, pp. 6909–6916, 2010.
[7] M. Zhao *et al*., "Mechanical and energy absorption characteristics of additively manufactured functionally graded sheet lattice structures with minimal surfaces," *Int. J. Mech. Sci.*, vol. 167, p. 105262, 2020.
[8] I. Maskery *et al*., "Insights into the mechanical properties of several triply periodic minimal surface lattice structures made by polymer additive manufacturing," *Polymer*, vol. 152, pp. 62–71, 2018.
[9] M. Sychov *et al*., "Mechanical properties of energy-absorbing structures with triply periodic minimal surface topology," *Acta Astronaut.*, vol. 150, pp. 81–84, 2018.
[10] M. Kurup and J. Pitchaimani, "Aeroelastic flutter of triply periodic minimal surface (TPMS) beams," *Compos. Part C: Open Access*, vol. 10, p. 100349, 2023.
[11] U. A. Simsek, C. E. Gayir, C. Basaran, and P. Sendur, "Modal characterization of additively manufactured TPMS structures: Comparison between different modeling methods," *Int. J. Adv. Manuf. Technol.*, vol. 115, pp. 657–674, 2020.
[12] N. Viet and W. Zaki, "Free vibration and buckling characteristics of functionally graded beams with triply periodic minimal surface architecture," *Compos. Struct.*, vol. 274, p. 114342, 2021.
[13] C. J. Ejeh, I. Barsoum, and R. K. A. Al-Rub, "Flexural properties of functionally graded additively manufactured AlSi10Mg TPMS latticed-beams," *Int. J. Mech. Sci.*, vol. 223, p. 107293, 2022.
[14] M. Afshar, A. P. Anaraki, and H. Montazerian, "Compressive characteristics of radially graded porosity scaffolds architectured with minimal surfaces," *Mater. Sci. Eng. C*, vol. 92, pp. 254–267, 2018.
[15] S. Ma *et al*., "Biological and mechanical property analysis for designed heterogeneous porous scaffolds based on the refined TPMS," *J. Mech. Behav. Biomed. Mater.*, vol. 107, p. 103727, 2020.
[16] H. N. Xuan *et al*., "Modelling of functionally graded triply periodic minimal surface (FG-TPMS) plates," *Compos. Struct.*, p. 116981, 2023.
[17] N. V. Nguyen *et al*., "An isogeometric analysis of functionally graded triply periodic minimal surface microplates," *Aerosp. Sci. Technol.*, vol. 137, p. 108270, 2023.
[18] F. Ebrahimi and E. Salari, "Size-dependent thermo-electrical buckling analysis of functionally graded piezoelectric nanobeams," *Smart Mater. Struct.*, vol. 24, no. 12, p. 125007, 2015.
[19] A. M. Zenkour and M. H. Aljadani, "Thermo-electrical buckling response of actuated functionally graded piezoelectric nanoscale plates," *Results Phys.*, vol. 13, p. 102192, 2019.
[20] A. Daneshmehr, A. Rajabpoor, and A. Hadi, "Size dependent free vibration analysis of nanoplates made of functionally graded materials based on nonlocal elasticity theory with high order theories," *Int. J. Eng. Sci.*, vol. 95, pp. 23–35, 2015.
[21] L. Gu, "Moving kriging interpolation and element-free Galerkin method," *Int. J. Numer. Methods Eng.*, vol. 56, no. 1, pp. 1–11, 2003.
[22] C. H. Thai *et al*., "An improved moving Kriging meshfree method for plate analysis using a refined plate theory," *Comput. Struct.*, vol. 176, pp. 34–49, 2016.
[23] C. H. Thai, V. N. V. Do, and H. N. Xuan, "An improved Moving Kriging-based meshfree method for static, dynamic and buckling analyses of functionally graded isotropic and sandwich plates," *Eng. Anal. Bound. Elem.*, vol. 64, pp. 122–136, 2016.
[24] T. N. Nguyen, C. H. Thai, and H. N. Xuan, "A novel computational approach for functionally graded isotropic and sandwich plate structures based on a rotation-free meshfree method," *Thin-Walled Struct.*, vol. 107, pp. 473–488, 2016.
[25] H. H. P. Dao *et al*., "Analysis of laminated composite and sandwich plate structures using generalized layerwise HSDT and improved meshfree radial point interpolation method," *Aerosp. Sci. Technol.*, vol. 58, pp. 641–660, 2016.
[26] T. N. Nguyen *et al*., "Geometrically nonlinear analysis of functionally graded material plates using an improved moving Kriging meshfree method based on a refined plate theory," *Compos. Struct.*, vol. 193, pp. 268–280, 2018.
[27] P. Lu *et al*., "Non-local elastic plate theories," *Proc. R. Soc. A Math. Phys. Eng. Sci.*, vol. 463, no. 2088, pp. 3225–3240, 2007.
[28] P. P. Van *et al*., "Small scale analysis of porosity-dependent functionally graded triply periodic minimal surface nanoplates using nonlocal strain gradient theory," *Appl. Math. Model.*, vol. 127, pp. 439–453, 2024.

Lieu Nguyen Thi Bich was born in Vietnam. She has a Ph.D. degree in Engineering Mechanics in 2019. Now, she is a lecturer at the Faculty of Civil Engineering, Ho Chi Minh City University of Technology and Education, Ho Chi Minh City, Vietnam. Her research interests are the computational mechanics, numerical methods for advanced materials.
Her email: lieuntb@hcmute.edu.vn. ORCID: https://orcid.org/0009-0000-4536-0526